



Published in final edited form as:

J Neural Eng. 2016 April ; 13(2): 026017. doi:10.1088/1741-2560/13/2/026017.

Individual Finger Control of the Modular Prosthetic Limb using High-Density Electrocorticography in a Human Subject

Guy Hotson^{#1,7}, David P McMullen^{#2}, Matthew S. Fifer³, Matthew S. Johannes⁴, Kapil D. Katyal⁴, Matthew P. Para⁴, Robert Armiger⁴, William S. Anderson², Nitish V. Thakor³, Brock A. Wester⁴, and Nathan E. Crone⁵

¹Department of Electrical and Computer Engineering, Johns Hopkins University, 3400 N Charles, Baltimore, MD 21218, USA

²Department of Neurosurgery, Johns Hopkins University, 600 N Wolfe, Baltimore, MD 21205, USA

³Department of Biomedical Engineering, Johns Hopkins University, 600 N Wolfe, Baltimore, MD 21205, USA

⁴Applied Neuroscience, JHU Applied Physics Laboratory, 7701 Montpelier Rd, Laurel, MD 20723, USA

⁵Department of Neurology, Johns Hopkins University, 600 N Wolfe, Baltimore, MD 21205, USA

These authors contributed equally to this work.

Abstract

Objective—We used native sensorimotor representations of fingers in a brain-machine interface to achieve immediate online control of individual prosthetic fingers.

Approach—Using high gamma responses recorded with a high-density ECoG array, we rapidly mapped the functional anatomy of cued finger movements. We used these cortical maps to select ECoG electrodes for a hierarchical linear discriminant analysis classification scheme to predict: 1) if any finger was moving, and, if so, 2) which digit was moving. To account for sensory feedback, we also mapped the spatiotemporal activation elicited by vibrotactile stimulation. Finally, we used this prediction framework to provide immediate online control over individual fingers of the Johns Hopkins University Applied Physics Laboratory (JHU/APL) Modular Prosthetic Limb (MPL).

Main Results—The balanced classification accuracy for detection of movements during the online control session was 92% (chance: 50%). At the onset of movement, finger classification was 76% (chance: 20%), and 88% (chance: 25%) if the pinky and ring finger movements were coupled. Balanced accuracy of fully flexing the cued finger was 64%, and 77% had we combined pinky and ring commands. Offline decoding yielded a peak finger decoding accuracy of 96.5% (chance: 20%) when using an optimized selection of electrodes. Offline analysis demonstrated significant finger-specific activations throughout sensorimotor cortex. Activations either prior to movement onset or during sensory feedback led to discriminable finger control.

⁷Author to whom any correspondence should be addressed. ; Email: Hotson.Guy@gmail.com, Phone: (650) 269-2165 .

Significance—Our results demonstrate the ability of ECoG-based BMIs to leverage the native functional anatomy of sensorimotor cortical populations to immediately control individual finger movements in real time.

1. Introduction

Brain-machine interfaces (BMIs) offer a promising approach for restoring function to patients with severe paralysis. By delivering direct cortical control over robotic prosthetic devices, BMIs could enable spinal cord injury (SCI) patients to perform activities of daily living (ADLs) necessary for self-sufficiency. However, many of these activities, such as preparing food or taking medications, require a level of hand dexterity that has yet to be achieved by BMIs. This dexterity can only be achieved by means of complex hand movements based on control of individual fingers. Decoding the neural correlates of finger control has been explored [1]–[6], but researchers have so far been unable to demonstrate online independent control of individual fingers.

To date, online cortical control of finger movements has only been achieved in the context of coordinated movements of multiple fingers. Electroencephalography (ECoG) signals recorded from sensorimotor areas have been used offline to reconstruct hand aperture [7] and classify different hand gestures [8]–[10]. ECoG has also been used online to continuously control grasping movements in parallel with arm movements [11], [12] and to classify different grasp types [9]. Neuronal firing rates from microelectrode arrays (MEAs) have also been used to achieve online cortical control over grasping in both nonhuman primates [13]–[16] and humans [17]–[19].

Offline decoding of single finger movements has been achieved with MEAs in non-human primates [2], [20], but MEA recordings in humans are rare and suffer from attrition of reliable single units over time [21]. Moreover, the restricted cortical areas covered by MEAs may not sufficiently sample the cortical networks of potential use in BMIs. Finger movements are represented in a larger area of sensorimotor cortex in humans than monkeys, and although there may be significant overlap in motor representations for individual fingers [22], [23], it is inherently difficult for MEA's to leverage what somatotopic organization is present.

In contrast, ECoG is able to deliver stable large-area coverage of sensorimotor areas [24], delivering control from multiple anatomical sites. For example, coverage of both arm and hand areas with a single ECoG grid enabled a subject to simultaneously control the ability to reach and grasp with a prosthetic limb [12]. This and other studies have chiefly used ECoG high gamma responses for online control. These spectral responses are robust enough to be detected in single trials, but because they reflect firing rate changes in populations of cortical neurons, their utility depends on the degree of functional segregation among these populations.

In spite of the evidence of limited finger somatotopy in motor cortex [22], [23], [25], both ECoG and fMRI studies have found a degree of separability in the peak population responses for different fingers in the precentral gyrus [26], [27]. These differential finger

responses have been used to perform offline classification and reconstruction of finger movements from ECoG recordings over sensorimotor areas [1], [3]. Offline classification between rest and four fingers (ignoring pinky) was near perfect in one subject in [9], though the system's performance dropped drastically when translated to an online grasp classification system synchronized to cue presentation. Additionally, several groups have performed offline regression of single finger movements [1], [4]–[6]. However, until now these achievements in offline classification and regression have not been translated into asynchronous (i.e., without knowledge of the cue) online control of individual fingers.

Here we show that high-density electrocorticography (ECoG) electrodes over sensorimotor areas can not only discriminate individual fingers offline, but that they can be used to asynchronously detect and classify finger movements online. A human subject demonstrated online control of the highly dexterous Modular Prosthetic Limb (MPL) [28]. The BMI relied only on the subject's cortical responses during movements of his corresponding native fingers, without extensive training or arbitrary mapping of user inputs to finger movements. Our approach of using the native functional anatomy of sensorimotor cortex obviates the need for operant conditioning, potentially providing immediate intuitive control to patients that can be expanded to a large number of degrees of freedom without placing significant cognitive burden on the patient. We performed further offline analysis to control for possible somatosensory feedback. These results demonstrate, for the first time, online control of individual fingers of a prosthetic hand, as well as offline analyses indicating a role for pre-movement signals in achieving this control.

2. Methods

2.1 Subject Info

The patient, a 20-year old right-handed male, underwent a left craniotomy for implantation of intracranial electrodes to localize the brain regions responsible for his seizures to guide resective surgery. These included a high-density 8×16 array of subdural electrodes (PMT Corp., Chanhassen, MN; 3mm center-to-center spacing, 1mm diameter) over sensorimotor regions. ECoG signals were recorded using distant standard subdural electrodes (2.3 mm diameter exposed) for ground and reference.

The subject gave informed consent for testing to be done according to a protocol approved by the Institutional Review Board of the Johns Hopkins Medical Institutions. Electrodes were localized with respect to cortical surface anatomy by volumetric co-registration of the subject's pre-implantation MRI with their post-surgical CT using the BioImage Suite [29]. This was used to help guide our electrode selection process for the BMI. After running the BMI, the reconstruction was checked against intraoperative photos from the implantation and explantation of the high density grid. The electrode locations on a two-dimensional snapshot of the reconstruction were manually adjusted relative to the underlying cortex via rotation, scaling, and translation of the grid to optimize the alignment between the grid and prominent gyral and sulcal landmarks present in both the 3D reconstruction and the intraoperative photos.

2.2. Offline Experimental Testing

A finger tapping task was performed to collect training data for the online finger decoder. Online BMI testing was performed the subsequent day. A passive vibration task and an additional finger tapping task were performed for offline analysis. Table 1 outlines the experiments performed. The tasks are described in more detail below.

2.2.1. Vibrotactile Stimulation—To investigate activation due to somatosensory feedback, we ran a vibrotactile stimulation experiment. While activation of post-central gyrus has been observed in paralyzed individuals [30] and able-bodied individuals during motor-imagery (without overt movement) [31]–[35], deafferented subjects lack cortical activation directly induced by somatosensory feedback. To address this, we used a vibrotactile stimulation experiment as a control. Vibrational motors were placed on the fingertips of the subject's right hand. The motors were turned on for 0.5 seconds every two seconds in a pseudorandom order by an Arduino microcontroller (Sparkfun Electronics, Boulder, CO) with two Adafruit v2.3 motor control shields (Adafruit Industries, New York City, NY). Each finger was vibrated 50 times, for a total of 250 trials.

2.2.2. Finger Tapping—The subject performed a visually cued finger tapping experiment. Trials were initiated by an experimenter on a presentation computer running psychtoolbox-3 [36] in MATLAB (MathWorks, Inc., Natick, MA, USA). After a trial was initiated, the system paused for two seconds, then displayed an image of a hand with one finger pseudo-randomly highlighted. The patient then alternately flexed and extended the corresponding finger on his right hand 5 times. Each finger was cued 25 times, for a total of 125 trials. Finger movements were recorded with a CyberGlove II (CyberGlove Systems LLC, San Jose, CA).

2.3. BMI Classifier Training

To perform online classifications of finger movements, we trained a hierarchical classifier on the offline finger tapping data. For any given time point, a binary linear discriminant analysis (LDA) classification was first used to determine if a movement was occurring. This allowed us to decode finger movements without synchronization to any cues (i.e. asynchronously). If a movement was detected, a classification from a second LDA classifier was used to determine which of the five fingers moved. The binary movement classifier was given a first-order Markovian transition probability; the prior for a prediction at time t was determined by the prediction at time $t-1$. These priors were calibrated online just before the online testing session to find a good tradeoff between false positives and false negatives.

To extract features for training the classifiers, we first re-referenced the high-density grid channels to a common average reference (CAR) with bad channels removed. The high gamma power was then extracted from each channel using the Hilbert transform with a flat-top Gaussian bandpass filter with cutoffs of 72 and 110 Hz using a 256 ms window and 128 ms step size. The average of the high gamma powers extracted from an 896 ms period before cue onset of each trial was used to gauge baseline activity for each electrode. The average of the high gamma power in an 896 ms period during finger movement of each trial was used to estimate activation due to the finger movement. This resulted in 125 feature vectors (one

for each trial) for both baseline and activation. These feature vectors were then used to train the movement detection and finger classification LDA classifiers.

When using the classifiers online, we used the same feature extraction workflow we used for training. To ensure smooth classifications, the features from the previous 50 samples were averaged at each time point. Due to slower computation speeds than anticipated, this resulted in a moving average of approximately 2.3 seconds of data to be used for classifications.

2.3. Online BMI Testing

When a finger movement was detected from the neural data, the corresponding MPL finger was commanded to flex at a fixed velocity. If a finger was not classified as moving, it was commanded to extend back towards the resting position at a fixed velocity. Before the online testing session began, the subject was given open use time and a practice session to acclimate to controlling the MPL fingers. During this acclimation period, the false positive rate of the movement classifier was tuned by adjusting the priors on the Markovian transition probabilities. The speed at which the fingers would flex/extend was also adjusted at this time, resulting in an extension velocity set to 40% of the flexion velocity. Figure 1 displays a flow diagram for the online BMI.

During the online testing session, the experimenter typically waited for all the MPL fingers to return to rest before initiating the next trial. There was a two second system pause before the appearance of the visual cue after trial initiation. This was used as a baseline (rest) period during post-hoc analysis.

2.4. BMI Control Evaluation

To evaluate the performance of the BMI control, we inspected the accuracy of the binary movement detection classifications and the 5-way individual finger classifications. Movement times relative to trial onsets were obtained from video analysis for trials where the subject's hand was visible. The proportion of movement vs non-movement predictions was binned in 250 ms bins relative to movement onset and averaged across trials. The proportion of movement predictions over time was used to evaluate the performance of the movement detection classifier.

The individual finger classifier performance was evaluated similarly by binning the single finger classifications that occurred when a movement was predicted. Because it was observed that the ring and little finger movements were often linked, the classification accuracy was calculated both considering them as the same and as separate fingers. Finger classification confusion matrices were calculated at the onset of peak movement detection, and during the time period where movements were most consistently predicted.

We also evaluated the global asynchronous finger classification performance. This was accomplished by calculating the accuracy of the individual finger classifier at any time a movement was predicted within seven seconds of cue onset. We also calculated the percentage of trials where the cued finger, and not any of the others, was fully flexed by the MPL. To find the balanced accuracy of flexing the cued finger, we averaged the accuracy of

fully flexing during the correct trial with the accuracy of not fully flexing during the incorrect trial.

To approximate the relative contributions of the electrodes to classification accuracies, we examined the cross-validated regularized LDA performance on its training data with varying numbers of electrodes.

2.5. Offline Analysis

Offline analysis was performed to determine the expected range of decoding performance with an optimized electrode selection during time periods preceding somatosensory feedback. While a lack of somatosensory feedback does not preclude activation of S1[37]–[39], direct cortical activation caused by somatosensory feedback is not present in deafferented patients in need of BMIs. We attempted to control for this by comparing the time course of finger-specific activation during the finger tapping and finger vibration tasks. We expect similar patterns of activation between paralyzed and able-bodied patients during the time period preceding somatosensory feedback, as suggested by the spatial patterns of activation seen in paralyzed patients during attempted movements [30]. The signals during this pre-sensory time period are likely representative of the minimum of what could be expected from paralyzed individuals for BMI control.

To view the time-course of activation relative to movement onset, the ECoG and CyberGlove data were segmented using the CyberGlove recordings. However, it was observed that the subject often initiated trials with a gross relaxation/extension movement of his hand and fingers before flexing the finger of interest. We therefore aligned the recordings separately to both the onset of any detected movement and the onset of flexion by the finger of interest. We then excluded any trial with more than a 400 ms disparity between the two alignment points, or excessive hand movements before onset of the finger movement; 19 trials were excluded in this way. The selection of onset times was verified by performing cross-validated LDA to predict which finger was moving using only the CyberGlove data (i.e., finger kinematics, not neural data). Chance levels were computed via permutation testing, and time points significantly above chance were detected via the Wilcoxon rank-sum test with a Bonferroni correction for multiple comparisons. We found the CyberGlove tracings of hand movement had differentiable features for different fingers during the preliminary hand movement (Supplementary Figure 1). We therefore aligned to our more conservative estimate of movement onset for all our subsequent offline analyses.

The conservative movement onset marker was used to compare the time course of activation during the finger tapping and vibration experiments. Spectrograms were created using the multitaper method from Chronux toolbox (<http://chronux.org>) with a window size of 128 ms, step size of 10 ms, passband of 16-160 Hz, cutoff frequencies of 10 Hz and 170 Hz, a time-bandwidth product of three, and five tapers.

We then investigated the time course of high gamma activation by using the same high gamma feature extraction method used for our online BMI. We removed visibly bad electrodes, CAR filtered the high-density grid electrodes, and used the Hilbert transform with a 72 to 110 Hz bandpass filter to compute the high gamma band power with a window

of 128 ms and a 16 ms step size. For every electrode in the motor and vibrotactile stimulation experiments, we only included activity during trials for the finger that evoked the strongest high gamma response. This allowed us to detect significant trial-averaged activations even if an electrode was only modulated by one finger. We then performed a Bonferroni corrected Wilcoxon rank-sum test for significant activation of high gamma relative to baseline at every point between 256 ms before and 240 ms after the onset of movement (or vibration, in the sensory trials). This allowed us to identify the earliest time points of cortical activation in each electrode for the motor and sensory task.

Finally, we investigated the time course of discriminable information between individual fingers during the motor and vibrotactile experiments. This was done to examine the decoding accuracy of finger movements during the period of time before finger-specific information was received through somatosensory feedback, which would not be present in deafferented subjects. The extracted high gamma features were smoothed using a 15th order moving average filter (window centers spanning 224 ms). We then performed 10-fold cross-validated LDA classification on the smoothed features; ten disjoint testing sets (each containing 10% of the trials) were each evaluated by (during each fold, separately) using the other 90% of the trials for feature selection and model training. The feature selection was performed using cross-validated regularization [40]. This regularization phase helped inform us as to what electrodes most consistently contributed to decoding performance. The number of times each electrode was chosen across the 10 folds of cross-validation was used as an index of its importance. We used extracted features in a causal manner, meaning that for a given time point t , features pertaining to that time point were extracted from windows which did not extend past t . This alignment was used to ensure our classifications were not dependent on future information, and therefore approximate the earliest time points when sensory feedback could have been included in the classifications. Feature extraction was repeated in a non-causal manner, aligned to the peak flexion time with a 30th order moving average filter (window centers spanning 464 ms) to estimate the upper limit on expected online decoding performance.

3. Results

3.1 BMI Electrode Selection

Preliminary inspection of high gamma activation during the motor task and vibrotactile stimulation, along with a preliminary reconstruction of the electrode locations, informed our feature selection process for the online decoder. Spectral features were used from a subset of electrodes that was chosen to avoid postcentral somatosensory cortex, though an error in the preliminary electrode localization led to the inclusion of two electrodes over postcentral gyrus. In training data from this subset of electrodes, cross-validated classification achieved 80% accuracy. Figure 2 depicts the locations of the electrodes chosen for the training set and for online BMI testing (below), as well as which electrodes showed significant activation during the motor and sensory tasks.

3.2. Online Testing

The subject performed 39 visually cued trials during online control of the MPL fingers (example performance, Supplementary Video 1). The subject began moving the prompted finger, on average, 1.43 seconds after cue onset.

Predictions were made at an average rate of 24 Hz. The average of the 50 most recently extracted spectral features was used for all predictions. This resulted in using the mean of features extracted over 2.34 seconds on average, with a group delay of approximately 1.17 seconds.

Figure 3 shows the accuracy of the binary movement classifier and the individual finger classifier as a function of time relative to cue onset. Movement detection accuracy reached a peak of 97%, sustained between 1.6 and 3.1 seconds after movement onset. Classifier accuracy during the baseline period was 87%, resulting in a balanced accuracy of 92%. Individual finger prediction accuracy peaked at 81% (chance 20%) when predicting which of all five fingers was moving, and 94% when classification for the ring and little finger was coupled (chance 25%).

At the onset of the peak movement detection period (1.6 seconds post-movement-onset), classification among all five fingers had an accuracy of 76%. When combining the ring and pinky fingers (they often moved together), accuracy was 88% (Figure 4, top row). The average classification accuracy during the peak movement detection period (1.6-3.1 seconds post-onset) was 67% for all five fingers, and 79% when combining ring and pinky fingers (Figure 4, middle row). The average accuracy at any time a movement was detected within seven seconds of trial onset (cue displayed) was 55% and 68% for five and four fingers, respectively (Figure 4, bottom row). Given that the accuracy in the baseline period was 87%, this equates to 60% and 72% accuracy for 6 and 5 class classifiers that include “rest” (chance levels of 17% and 20%, respectively).

The balanced accuracy of flexing the cued MPL finger (within seven seconds of trial onset) was 64%, and 77% when pinky and ring positions were summed together. The cued finger was the only finger fully flexed by the MPL during 43% of the trials, and 62% when pinky and ring commands were combined. The average traces of the normalized MPL finger positions during their respectively cued trials are shown in Figure 5. The dashed lines represent the average position of the other four fingers during that trial (e.g. the solid blue line depicts the thumb, while the dashed blue line depicts the mean position of the other fingers during thumb trials).

A cross-validated, regularized parameter search limited to the electrodes selected for the online BMI revealed that adding five electrodes (shown in Figure 2) led to the greatest reductions in error on the training data, and the addition of other electrodes typically increased error. In spite of excluding electrodes identified by preliminary electrode localization as being over the postcentral gyrus, the four electrodes which contributed the most to decoding accuracy all showed significant activation during the vibration task. We therefore performed offline analyses to investigate the motor decoding results when controlling for the contributions of somatosensory cortex activity.

3.3. Offline Analysis

To investigate the relative contributions of somatosensory and motor cortex to the BMI, we compared the spatiotemporal patterns of activation during offline passive vibrotactile stimulation vs. finger movement. Figure 6 shows spectral activation during passive vibration and offline finger movement in the two electrodes that contributed most to online decoding performance. Intensities are saturated to better see the earliest activation times.

A total of 33 electrodes displayed significant task-related spectral modulation during finger movement in the 512 ms centered on movement onset. These electrodes crossed significance thresholds a median of 16 ms before onset of movement. The 25 electrodes with significant modulation in the 512 ms centered on vibrotactile stimulus onset reached significance a median of 80 ms after vibration onset. This suggests that a good deal of the activation during finger movements was not solely due to somatosensory feedback.

Spectral modulations during the motor task significantly exceeded baseline levels in four of the five electrodes that contributed most to the classifier performance. In these electrodes, activation first became significant during feature extraction windows (256 ms long) centered 16, 48, 128, and 160 ms *before* the onset of movement (one did not display significant activation). In the sensory task, activation first reached significance 48 ms *after* the onset of vibration in three of the five electrodes, 64 ms in one electrode, and never in one electrode.

To investigate the ability of early motor-related spectral modulations to discriminate between fingers, we built and tested classifiers throughout the time course of the finger movement task and passive finger vibrations. Supplementary Figure 2 displays finger classification accuracies over time relative to the movements recorded by their respective finger sensors in the CyberGlove. Prediction of thumb movements was particularly early and robust. Figure 7 shows the electrodes selected during the regularization phase. The size of the red circle for each electrode represents how often that electrode was selected during regularization across the ten folds of cross-validation. A high degree of overlap was found between the most important electrodes during the sensory and motor tasks, though additional precentral electrodes were selected for decoding early in the motor task.

Mean classification accuracy is shown for motor task and vibrotactile stimulation in Figure 8. Time points were referenced to the onset of any detected movement (via CyberGlove) or the onset of vibration. At each time point, the mean of the previous 15 feature extraction windows was used for cross-validated classification. This causal decoding scheme made use of the 352 ms of data preceding each time point. Classification accuracy during the finger tapping task was significantly higher than the corresponding accuracy during vibrotactile stimulation between -32 ms to 224 ms ($p < 0.05$, Wilcoxon rank sum, Bonferroni corrected for 30 comparisons). The classification accuracy for finger vibration exceeded chance 192 ms after stimulation onset. The mean classification accuracy during the motor task reached 70.7% at the corresponding time of 192 ms after movement onset. Decoding based on the ECoG signals showed similar accuracy over time relative to using the CyberGlove recordings for finger decoding. This was in spite of the fact that the ECoG features were associated with a group delay of 184 ms, whereas CyberGlove relied only on the instantaneous time value.

While peak performance without somatosensory feedback cannot be reliably ascertained from this data, the time course of classification accuracies indicate that accuracy using signals only related to motor function (without accuracy inflated by sensory feedback not present in paralyzed subjects) would likely achieve at least 70.7% accuracy in discriminating which finger was being moved. When data was aligned to the peak flexion time and the smoothing window was increased to 480 ms, we obtained a maximum accuracy of 96.5% and a mean accuracy of 90.2% between 190 ms before to 1250 ms after the peak flexion (after correcting for group delays). Based on these findings, we estimate that a high-density ECoG array over sensorimotor areas would yield individual finger classification accuracies in the range of 70.7-96.5% using motor signals in the deafferented patient population that would benefit most from invasive BMI systems.

4. Discussion

We have demonstrated, for the first time in humans, online neural decoding of individual finger movements to control a dexterous modular prosthetic limb. We utilized high gamma power extracted from a high-density ECoG grid situated over a subject's sensorimotor cortex to produce intuitive BMI finger control. This was accomplished without arbitrary mappings of user inputs or extensive training by using the native cortical representations of finger movements. During online control, we utilized all available neural information in a subset of electrodes to produce highly accurate control of fingers. For further offline analysis, we limited our analysis to time periods preceding discriminable sensory afferent information to more closely mimic SCI patients' neural activity. We found this still yielded discriminable information useful for finger control.

We were able to accurately decode finger flexions online using the native sensorimotor representations of fingers in the brain. The classification accuracy for the online BMI at the onset of the most reliable time period for detecting movements (1.6 seconds post-cue) was 76% (88% with ring and pinky combined). The balanced accuracy of correctly flexing the cued MPL finger was 64% (77% with ring/pinky combined). Our asynchronous binary prediction of whether the subject was moving any finger yielded a balanced accuracy of 92%. To our knowledge, this is the first online demonstration by a human subject of neural control of individual finger flexion with a robotic prosthetic limb. We further believe that the control of five individual fingers in this study marks the greatest number of distinct degrees of freedom controlled online with ECoG signals. By accomplishing this without the need for operant conditioning, we have shown that high density ECoG can leverage the native somatotopy of individual fingers to provide patients with immediate, more intuitive finger control.

Our online results contribute to the growing literature of online ECoG control over robotic prosthetics. Subjects have used ECoG to asynchronously modulate the aperture of two grasp types (77% of trials correct to completion) while simultaneously controlling elbow movements (34% of trials correct to completion) with a prosthetic limb [11]. The ability to simultaneously control reach and grasp independently with a prosthetic limb was demonstrated with mean accuracies of 84% and 81% for reach and grasp respectively [12]. ECoG control signals have been further integrated with intelligent robotics to pick up and

move objects with a mean success rate of 70% [41]. Yanagisawa et al. was able to asynchronously detected hand movements (61% detected within one second) then decode which of three different hand movements was performed (69.2% accuracy) [42]. Chestek et al. showed 97% accuracy in classifying between resting and grasping at a fixed time relative to cue in two subjects [9]. Their accuracy was 57% in one subject when expanded to two different grasp types vs rest, and 55% accuracy in another subject when classifying between rest and four grasp types. ECoG signals from hand somatosensory areas were also used in [43], where attempted thumb, wrist, and elbow movements were used as control signals for 3D arm position. Their subject achieved 80% accuracy in a 3D cursor task leading up to their MPL endpoint control, demonstrating the ability of postcentral hand area ECoG signals recorded from a paralyzed subject to control a BMI. Our online asynchronous classification accuracies of 64% and 77% for rest vs five and four fingers respectively build on the previous literature to show, for the first time, that neural recordings can be used to provide immediate online control of individual fingers without the need for operant conditioning.

In order to more closely mimic the neural activity of an SCI patient, we performed further offline analyses where we limited neural activity to time periods preceding sensory feedback. Slight pre-trial movements of our subject's hands led to loss of data from conservative estimates of movement onset determination. While cortical reorganization occurs after SCI/amputation, multiple groups have demonstrated continued sensorimotor activity during imagined or triggered phantom hand movements [44]–[47]. We believe SCI patients could harness this continued neural activity to control a robotic limb BMI. Indeed, groups working with a SCI patient implanted with ECoG have demonstrated SCI patients' ability to modulate this rhythms to control a BMI [43]. In spite of the very conservative estimate of movement onset, spectrograms of high gamma activation revealed significant pre-movement activity (Figure 6). We estimate a lower bound of 70.7% decoding accuracy without sensory feedback. Higher single finger decoding accuracies at movement onset was previously found [1], but this was achieved with a non-causal methodology that did not account for sensory feedback. Our peak accuracy during offline analysis of the motor task reached 96.5%, with a mean accuracy of over 90% during a time period lasting over a second. This establishes an upper bound of over 90% for expected online single finger decoding accuracy using high-definition ECoG over sensorimotor areas. A comparable drop in performance was seen previously [9] when predictions were only made using data from before movement onset. This is consistent with our estimate of the expected lower bound accuracy.

Our analysis revealed widespread pre-movement activity across both precentral and, interestingly, postcentral gyri during the finger tapping task. Much of our decoding accuracy was derived from electrodes that also showed activation during vibrotactile stimulation (Figure 7). This may have been due in part to the high-density grid having better coverage of the finger representation on the postcentral gyrus than the precentral gyrus. Another possible reason the somatosensory-modulated electrodes were essential to decoding can be traced to more distinct somatotopy of individual fingers in the postcentral gyrus than in the precentral gyrus [22], [23], [25], [48], [49]. A large portion of the post-movement activity detected in postcentral gyrus was no doubt the result of afferent cutaneous and proprioceptive information. However, it is possible that a subset of the pre-movement activity in this region

was the result of an “efference copy” sent from premotor and associated motor planning cortices [32], [50], [51]. These results are similar to a human ECoG study that showed pre-movement signals in sensory areas that were led by signals in task-related areas in premotor cortices [52]. This movement-related activation, observed in both pre- and postcentral cortex, has been noted in paralyzed subjects [37]–[39]. Furthermore, postcentral activity was recently used to provide control over a three dimensional brain-machine interface to a paralyzed subject [43].

Further advancements in ours and other systems are necessary before BMIs will be able to meet the clinical needs of SCI patients. Although we were able to demonstrate immediate robust online control of individual fingers, future users will need more accurate systems before they can perform the ADLs necessary for full autonomy. However, while the raw decoding accuracy found in this study would not meet the performance requirements of a functionally useful prosthetic device, cortical adaptation has been shown to increase BMI performance over time [53]–[55]. This would likely improve results for patients that can work with the BMI system longer than the brief testing session performed in this study. Additionally, decoding from more comprehensive coverage of precentral areas would likely further improve system robustness [1], [9]. Finally, other avenues of research may also create more functionally useful BMIs. Incorporating intelligent robotics into neural-only BMIs may allow users to perform a wide variety of tasks [41], [56]. By using environmental sensors to inform the system of which fingers the user likely wants to flex, the system could incorporate prior knowledge of grasp trajectories to accomplish advanced tasks in the presence of noisy cortical control signals.

5. Conclusions

We demonstrated the ability of a patient implanted with high density ECoG over sensorimotor areas to asynchronously control individual finger movements intuitively in an online BMI, without the need for online training sessions. Offline analysis showed a large amount of the decoding accuracy in our coverage area was derived from postcentral gyrus. While our online control was likely highly influenced by sensory feedback, we found that the signals in somatosensory areas showed significant activation before movement onset, which might still occur in patients lacking afferent somatosensory inputs. Furthermore, decoding accuracy over the course of the movement mirrored the separability of hand positions—the more the CyberGlove recordings became identifiable as a specific finger movement, the more the finger movement could be decoded from the preceding window of neural data. Our findings support previous studies suggesting an efference copy activating somatosensory cortex [32], [50], [51]. Here we demonstrated that this information can be used to control individual fingers in an able-bodied subject. Future studies will need to determine whether the same or similar signals can be used in paralyzed patient populations, but recent work has demonstrated promising results showing sensorimotor activation in deafferented patients [37]–[39], [43].

We have demonstrated, for the first time, online control of all five individual fingers of a robotic prosthetic hand independently and hope that insights from this study can one day be applied to paralyzed patient populations to enable them to perform dexterous ADLs.

Supplementary Material

Refer to Web version on PubMed Central for supplementary material.

Acknowledgements

The Authors would like to thank G. Milsap for assistance with experimental testing, G. Milsap, Y. Wang, K. Rupp, and A. Korzeniewska for lab meeting discussions of our approach and analysis. The authors would like to thank John Roycroft and John Helder for their help with configuring the MPL systems for development, experimentation, and data acquisition. This work was funded by the National Institutes of Health (NIH) through a National Institute of Neurological Disorders and Stroke (NINDS) grant 1R01NS088606-01.

References

- [1]. Kubanek J, Miller KJ, Ojemann JG, Wolpaw JR, Schalk G. Decoding flexion of individual fingers using electrocorticographic signals in humans. *J Neural Eng.* Dec.2009 6(no. 6):66001.
- [2]. Acharya S, Tenore F, Aggarwal V, Etienne-Cummings R, Schieber MH, Thakor NV. Decoding individuated finger movements using volume-constrained neuronal ensembles in the M1 hand area. *IEEE Trans. Neural Syst. Rehabil. Eng.* Feb.2008 16(no. 1):15–23. [PubMed: 18303801]
- [3]. Wang, W.; Degenhart, AD.; Collinger, JL.; Vinjamuri, R.; Sudre, GP.; Adelson, PD.; Holder, DL.; Leuthardt, EC.; Moran, DW.; Boninger, ML.; Schwartz, AB.; Crammond, DJ.; Tyler-Kabara, EC.; Weber, DJ. Human motor cortical activity recorded with micro-ECOG electrodes during individual finger movements. *Conf. Proc. Annu. Int. Conf. IEEE Eng. Med. Biol. Soc. IEEE Eng. Med. Biol. Soc. Conf.*; 2009. p. 586-589.
- [4]. Flamary R, Rakotomamonjy A. Decoding finger movements from ECoG signals using switching linear models. *Front. Neurosci.* Mar.2012 6
- [5]. Liang N, Bougrain L. Decoding finger flexion from band-specific ECoG signals in humans. *Front. Neurosci.* Jun.2012 6
- [6]. Nakanishi Y, Yanagisawa T, Shin D, Chen C, Kambara H, Yoshimura N, Fukuma R, Kishima H, Hirata M, Koike Y. Decoding fingertip trajectory from electrocorticographic signals in humans. *Neurosci. Res.* Aug.2014 85:20–27. [PubMed: 24880133]
- [7]. Acharya S, Fifer MS, Benz HL, Crone NE, Thakor NV. Electrocorticographic amplitude predicts finger positions during slow grasping motions of the hand. *J. Neural Eng.* Aug.2010 7(no. 4): 046002. [PubMed: 20489239]
- [8]. Pistohl T, Schulze-Bonhage A, Aertsen A, Mehring C, Ball T. Decoding natural grasp types from human ECoG. *NeuroImage.* Jan.2012 59(1):248–260. [PubMed: 21763434]
- [9]. Chestek CA, Gilja V, Blabe CH, Foster BL, Shenoy KV, Parvizi J, Henderson JM. Hand posture classification using electrocorticography signals in the gamma band over human sensorimotor brain areas. *J. Neural Eng.* Apr.2013 10(no. 2):026002. [PubMed: 23369953]
- [10]. Bleichner MG, Freudenburg ZV, Jansma JM, Aarnoutse EJ, Vansteensel MJ, Ramsey NF. Give me a sign: decoding four complex hand gestures based on high-density ECoG. *Brain Struct. Funct.* Oct.2014 :1–14.
- [11]. Yanagisawa T, Hirata M, Saitoh Y, Kishima H, Matsushita K, Goto T, Fukuma R, Yokoi H, Kamitani Y, Yoshimine T. Electrocorticographic control of a prosthetic arm in paralyzed patients. *Ann. Neurol.* Mar.2012 71(no. 3):353–361. [PubMed: 22052728]
- [12]. Fifer MS, Hotson G, Wester B, McMullen DP, Wang Y, Johannes MS, Katyal KD, Helder JB, Para MP, Vogelstein RJ, Anderson WS, Thakor NV, Crone NE. Simultaneous neural control of simple reaching and grasping with the modular prosthetic limb using intracranial EEG. *IEEE Trans. Neural Syst. Rehabil. Eng.* May; 2014 22(no. 3):695–705. [PubMed: 24235276]
- [13]. Carmena JM, Lebedev MA, Crist RE, O’Doherty JE, Santucci DM, Dimitrov DF, Patil PG, Henriquez CS, Nicolelis MAL. Learning to control a brain-machine interface for reaching and grasping by primates. *PLoS Biol.* Nov.2003 1(no. 2):E42. [PubMed: 14624244]

- [14]. Kim HK, Biggs SJ, Schloerb DW, Carmena JM, Lebedev MA, Nicolelis MAL, Srinivasan MA. Continuous shared control for stabilizing reaching and grasping with brain-machine interfaces. *IEEE Trans. Biomed. Eng.* Jun.2006 53(no. 6):1164–1173. [PubMed: 16761843]
- [15]. Velliste M, Perel S, Spalding MC, Whitford AS, Schwartz AB. Cortical control of a prosthetic arm for self-feeding. *Nature.* Jun.2008 453(no. 7198):1098–101. [PubMed: 18509337]
- [16]. Zhuang J, Truccolo W, Vargas-Irwin C, Donoghue JP. Decoding 3-D reach and grasp kinematics from high-frequency local field potentials in primate primary motor cortex. *IEEE Trans. Biomed. Eng.* Jul.2010 57(no. 7):1774–1784. [PubMed: 20403782]
- [17]. Hochberg LR, Bacher D, Jarosiewicz B, Masse NY, Simeral JD, Vogel J, Haddadin S, Liu J, Cash SS, van der Smagt P, Donoghue JP. Reach and grasp by people with tetraplegia using a neurally controlled robotic arm. *Nature.* May; 2012 485(no. 7398):372–375. [PubMed: 22596161]
- [18]. Collinger JL, Wodlinger B, Downey JE, Wang W, Tyler-Kabara EC, Weber DJ, McMorland AJ, Velliste M, Boninger ML, Schwartz AB. High-performance neuroprosthetic control by an individual with tetraplegia. *The Lancet.* Feb.2013 381(no. 9866):557–564.
- [19]. Wodlinger B, Downey JE, Tyler-Kabara EC, Schwartz AB, Boninger ML, Collinger JL. Ten-dimensional anthropomorphic arm control in a human brain-machine interface: difficulties, solutions, and limitations. *J. Neural Eng.* Feb.2015 12(no. 1):016011. [PubMed: 25514320]
- [20]. Hamed SB, Schieber MH, Pouget A. Decoding M1 neurons during multiple finger movements. *J. Neurophysiol.* Jul.2007 98(no. 1):327–333. [PubMed: 17428905]
- [21]. Vaidya, M.; Dickey, A.; Best, MD.; Coles, J.; Balasubramanian, K.; Suminski, AJ.; Hatsopoulos, NG. Ultra-Long Term Stability of Single Units Using Chronically Implanted Multielectrode Arrays. *Conf. Proc. Annu. Int. Conf. IEEE Eng. Med. Biol. Soc. IEEE Eng. Med. Biol. Soc. Annu. Conf.*; 2014. p. 4872-4875.
- [22]. Sanes JN, Donoghue JP, Thangaraj V, Edelman RR, Warach S. Shared neural substrates controlling hand movements in human motor cortex [see comments]. *Science.* 1995; 268:1775–1777. [PubMed: 7792606]
- [23]. Schieber MH, Hibbard LS. How somatotopic is the motor cortex hand area? *Science.* 1993; 261:489–492. [PubMed: 8332915]
- [24]. Chao ZC, Nagasaka Y, Fujii N. Long-Term Asynchronous Decoding of Arm Motion Using Electrographic Signals in Monkeys. *Front. Neuroengineering.* Mar.2010 3
- [25]. Schieber MH. Constraints on somatotopic organization in the primary motor cortex. *J. Neurophysiol.* Nov.2001 86(no. 5):2125–2143. [PubMed: 11698506]
- [26]. Siero JCW, Hermes D, Hoogduin H, Luijten PR, Ramsey NF, Petridou N. BOLD matches neuronal activity at the mm scale: A combined 7 T fMRI and ECoG study in human sensorimotor cortex. *NeuroImage.* Nov.2014 101:177–184. [PubMed: 25026157]
- [27]. Miller KJ, Zanos S, Fetz EE, den Nijs M, Ojemann JG. Decoupling the cortical power spectrum reveals real-time representation of individual finger movements in humans. *J. Neurosci. Off. J. Soc. Neurosci.* Mar.2009 29(no. 10):3132–3137.
- [28]. Johannes MS, Bigelow JD, Burck JM, Harshbarger SD, Kozlowski MV, Van Doren T. An overview of the developmental process for the modular prosthetic limb. *Johns Hopkins APL Tech. Dig.* 2011; 30(no. 3):207–216.
- [29]. Duncan JS, Papademetris X, Yang J, Jackowski M, Zeng X, Staib LH. Geometric strategies for neuroanatomic analysis from MRI. *NeuroImage.* 2004; 23(Suppl 1):S34–45. [PubMed: 15501099]
- [30]. Kokotilo KJ, Eng JJ, Curt A. Reorganization and Preservation of Motor Control of the Brain in Spinal Cord Injury: A Systematic Review. *J. Neurotrauma.* Nov.2009 26(no. 11):2113–2126. [PubMed: 19604097]
- [31]. Miller KJ, Schalk G, Fetz EE, den Nijs M, Ojemann JG, Rao RPN. Cortical activity during motor execution, motor imagery, and imagery-based online feedback. *Proc. Natl. Acad. Sci.* Feb.2010 : 200913697.
- [32]. Christensen MS, Lundbye-Jensen J, Geertsen SS, Petersen TH, Paulson OB, Nielsen JB. Premotor cortex modulates somatosensory cortex during voluntary movements without proprioceptive feedback. *Nat. Neurosci.* Apr.2007 10(no. 4):417–419. [PubMed: 17369825]

- [33]. Porro CA, Francescato MP, Cettolo V, Diamond ME, Baraldi P, Zuiani C, Bazzocchi M, di Prampero PE. Primary motor and sensory cortex activation during motor performance and motor imagery: a functional magnetic resonance imaging study. *J. Neurosci.* 1996; 16:7688–7698. [PubMed: 8922425]
- [34]. Lacourse MG, Orr ELR, Cramer SC, Cohen MJ. Brain activation during execution and motor imagery of novel and skilled sequential hand movements. *NeuroImage.* Sep.2005 27(no. 3):505–519. [PubMed: 16046149]
- [35]. Felton EA, Wilson JA, Williams JC, Garell PC. Electrocorticographically controlled brain–computer interfaces using motor and sensory imagery in patients with temporary subdural electrode implants. *J. Neurosurg.* Mar.2007 106(no. 3):495–500. [PubMed: 17367076]
- [36]. Brainard DH. The Psychophysics Toolbox. *Spat. Vis.* Jan.1997 10(no. 4):433–436. [PubMed: 9176952]
- [37]. Shoham D, Grinvald A. The cortical representation of the hand in macaque and human area S-I: high resolution optical imaging. *J. Neurosci.* Sep.2001 21(no. 17):6820–6835. [PubMed: 11517270]
- [38]. Hotz-Boendermaker S, Funk M, Summers P, Brugger P, Hepp-Reymond M-C, Curt A, Kollias SS. Preservation of motor programs in paraplegics as demonstrated by attempted and imagined foot movements. *NeuroImage.* Jan.2008 39(no. 1):383–394. [PubMed: 17919932]
- [39]. Cramer SC, Lastra L, Lacourse MG, Cohen MJ. Brain motor system function after chronic, complete spinal cord injury. *Brain.* Dec.2005 128(no. 12):2941–2950. [PubMed: 16246866]
- [40]. Guo Y, Hastie T, Tibshirani R. Regularized linear discriminant analysis and its application in microarrays. *Biostatistics.* Jan.2007 8(no. 1):86–100. [PubMed: 16603682]
- [41]. McMullen D, Hotson G, Katyal K, Wester B, Fifer M, McGee T, Harris A, Johannes M, Vogelstein RJ, Ravitz A, Anderson W, Thakor N, Crone N. Demonstration of a semi-autonomous hybrid brain-machine interface using human intracranial EEG, eye tracking, and computer vision to control a robotic upper limb prosthetic. *IEEE Trans. Neural Syst. Rehabil. Eng.* 2014 Early Access Online.
- [42]. Yanagisawa T, Hirata M, Saitoh Y, Goto T, Kishima H, Fukuma R, Yokoi H, Kamitani Y, Yoshimine T. Real-time control of a prosthetic hand using human electrocorticography signals. *J. Neurosurg.* Jun.2011 114(no. 6):1715–1722. [PubMed: 21314273]
- [43]. Wang W, Collinger JL, Degenhart AD, Tyler-Kabara EC, Schwartz AB, Moran DW, Weber DJ, Wodlinger B, Vinjamuri RK, Ashmore RC, Kelly JW, Boninger ML. An electrocorticographic brain interface in an individual with tetraplegia. *PLoS ONE.* Feb.2013 8(no. 2):e55344. [PubMed: 23405137]
- [44]. Mercier C, Reilly KT, Vargas CD, Aballea A, Sirigu A. Mapping phantom movement representations in the motor cortex of amputees. *Brain.* Aug.2006 129(no. 8):2202–2210. [PubMed: 16844715]
- [45]. Reilly KT, Mercier C, Schieber MH, Sirigu A. Persistent hand motor commands in the amputees' brain. *Brain.* Aug.2006 129(no. 8):2211–2223. [PubMed: 16799174]
- [46]. Erslund L, Rosén G, Lundervold A, Smievoll AI, Tillung T, Åkan Sundberg H. Phantom limb imaginary fingertapping causes primary motor cortex activation: an fMRI study. *Neuroreport.* 1996; 8(no. 1):207–210. others. [PubMed: 9051782]
- [47]. Alkadhi H, Brugger P, Boendermaker SH, Crelier G, Curt A, Hepp-Reymond M-C, Kollias SS. What Disconnection Tells about Motor Imagery: Evidence from Paraplegic Patients. *Cereb. Cortex.* Feb.2005 15(no. 2):131–140. [PubMed: 15238440]
- [48]. Nelson AJ, Chen R. Digit somatotopy within cortical areas of the postcentral gyrus in humans. *Cereb. Cortex.* Oct.2008 18(no. 10):2341–2351. [PubMed: 18245039]
- [49]. Powell TP, Mountcastle VB. Some aspects of the functional organization of the cortex of the postcentral gyrus of the monkey: a correlation of findings obtained in a single unit analysis with cytoarchitecture. *Bull. Johns Hopkins Hosp.* Sep.1959 105:133–162. [PubMed: 14434571]
- [50]. Crapse TB, Sommer MA. Corollary discharge circuits in the primate brain. *Curr. Opin. Neurobiol.* Dec.2008 18(no. 6):552–557. [PubMed: 18848626]

- [51]. Gritsenko V, Krouchev NI, Kalaska JF. Afferent input, efference copy, signal noise, and biases in perception of joint angle during active versus passive elbow movements. *J. Neurophysiol.* Sep. 2007 98(no. 3):1140–1154. [PubMed: 17615137]
- [52]. Sun FT, Morrell MJ, Wharen RE. Responsive cortical stimulation for the treatment of epilepsy. *Neurother. J. Am. Soc. Exp. Neurother.* 2008; 5(no. 1):68–74.
- [53]. Ganguly K, Carmena JM. Emergence of a stable cortical map for neuroprosthetic control. *PLoS Biol.* Jul.2009 7(no. 7):e1000153. [PubMed: 19621062]
- [54]. Lebedev MA, Carmena JM, O’Doherty JE, Zacksenhouse M, Henriquez CS, Principe JC, Nicolelis MAL. Cortical Ensemble Adaptation to Represent Velocity of an Artificial Actuator Controlled by a Brain-Machine Interface. *J. Neurosci.* May; 2005 25(no. 19):4681–4693. [PubMed: 15888644]
- [55]. Rouse AG, Williams JJ, Wheeler JJ, Moran DW. Cortical Adaptation to a Chronic Micro-Electrocorticographic Brain Computer Interface. *J. Neurosci.* Jan.2013 33(no. 4):1326–1330. [PubMed: 23345208]
- [56]. Muelling K, Venkatraman A, Valois J-S, Downey J, Weiss J, Javdani S, Hebert M, Schwartz AB, Collinger JL, Bagnell JA. Autonomy Infused Teleoperation with Application to BCI Manipulation. *ArXiv Prepr.* 2015 ArXiv150305451.

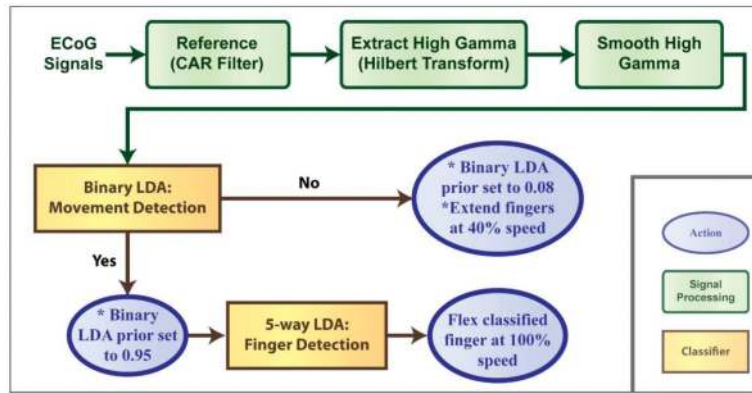


Figure 1. Flow diagram of the online BMI processing. Signals are rereferenced, high gamma is extracted and smoothed, and then a hierarchical classifier is used to determine if/which fingers should be moved.

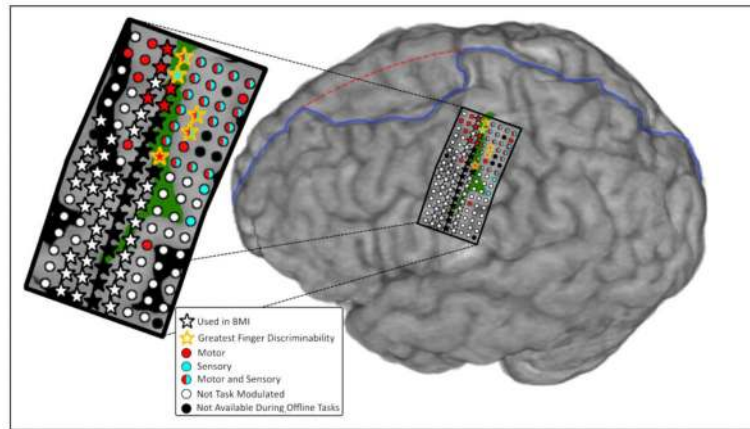


Figure 2.

Electrodes used for online BMI. Starred electrodes were selected for online BMI control. Sulci are accentuated in the inset for improved visibility, with the central sulcus highlighted in green. Post-hoc analysis showed the electrodes with gold stars contributed the most to decoding accuracy on the training set. Light blue electrodes showed significant activation during vibrotactile stimulation, and red electrodes were active during the motor task. The electrodes that were not available for the offline analysis are filled black. Purple outlines the interhemispheric fissure and red outlines the previously resected superior frontal gyrus.

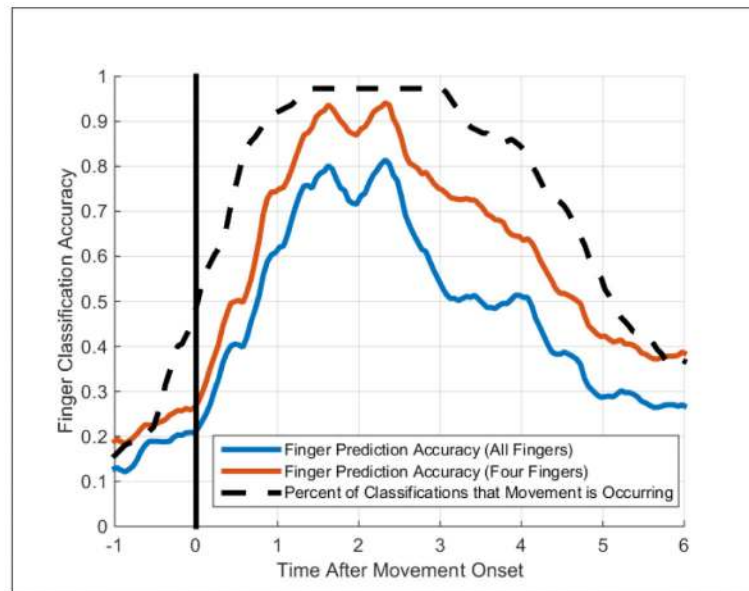


Figure 3. Classification accuracies over time for movement and finger classification. Classifications were aggregated in 250 ms time bins, and accuracies were averaged across trials. The black dashed line depicts the average proportion of predictions that a window contained movement (i.e., versus rest). The solid black vertical line depicts movement onset.

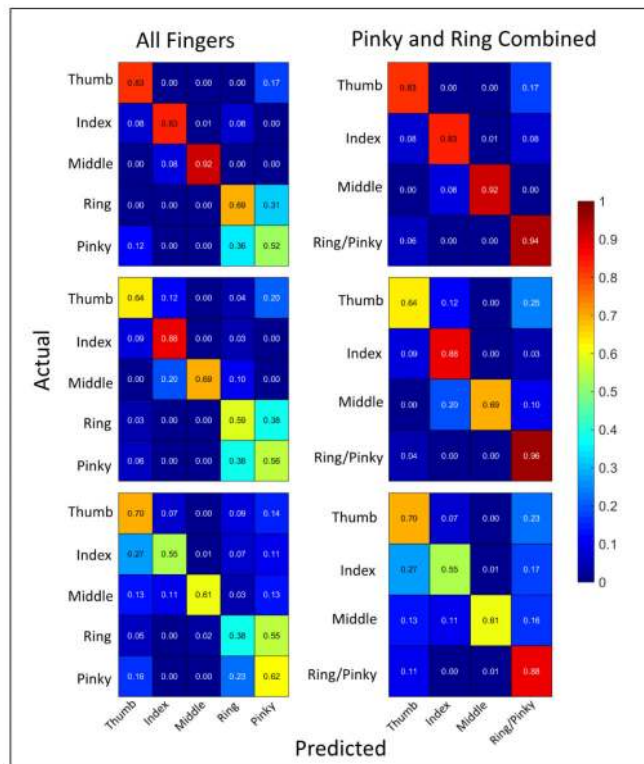


Figure 4. Confusion matrices for finger classifications. The left column of matrices shows results for all five fingers, the right column shows results with pinky and ring fingers combined. The top row depicts the confusion matrices at the onset of the peak movement classification time, middle shows the average over the 1.5 seconds of peak movement detection time, and the bottom is any time within seven seconds of cue onset.

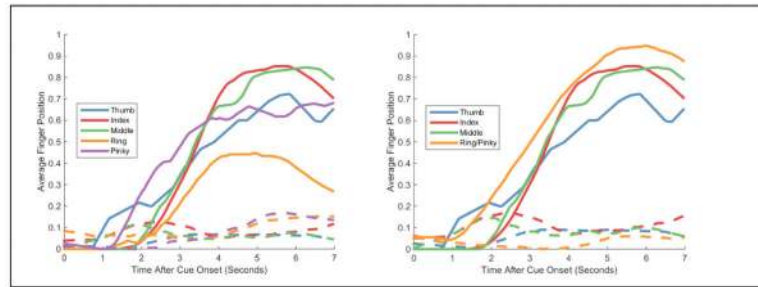


Figure 5.

Average normalized MPL finger position of all five fingers during online BMI control (left), and with ring and pinky commands aggregated (orange, right). Solid lines depict the average position of the cued finger as a proportion of maximum flexion, where 1 corresponds to fully flexed and 0 corresponds to fully extended. The corresponding dashed lines show the average position of all the other fingers during the cued finger's trials.

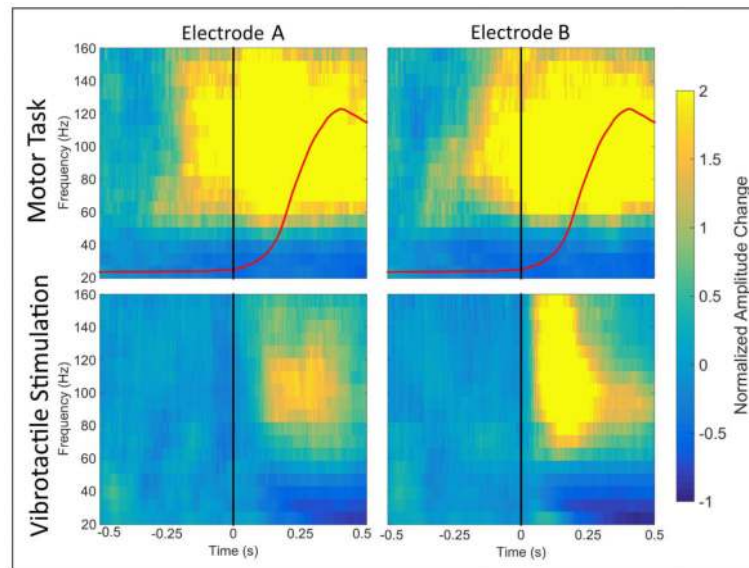


Figure 6. Spectral activation during offline index finger tapping (top) and passive index finger vibration (bottom) for the two BMI electrodes that contributed most to performance with the training data. For finger tapping (top row) the solid black line marks the onset ($t=0$) of any hand movement detected by the CyberGlove. The red curve is the average trace of the index finger sensors on the CyberGlove. For finger vibration (bottom row), the black line marks onset of the vibratory stimulus. Activation significantly exceeded baseline levels 160 ms and 48 ms before movement onset during the motor task (top row), and 48 ms after the onset of vibrotactile stimulation (bottom row).

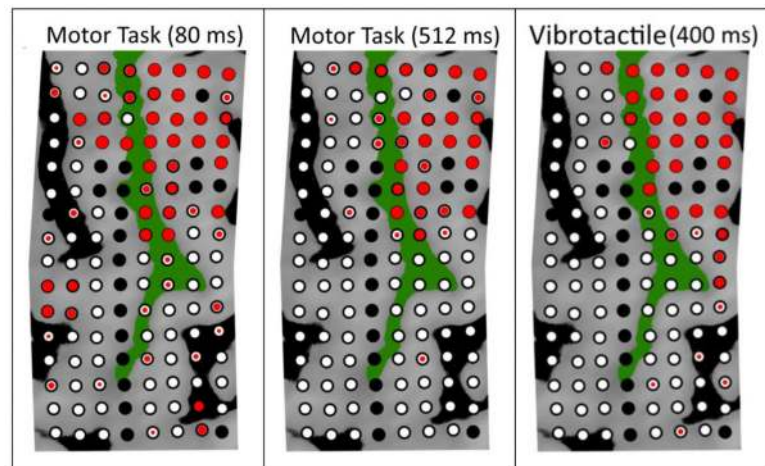


Figure 7.

Electrodes most consistently selected during the ten folds of cross-validation for the offline motor and sensory task classifications. Green denotes the central sulcus with the left side of every image being anterior and right being posterior. Cross-validated regularization was performed on the training data during classification at every time step. Size of the red circle corresponds to the frequency with which electrodes were selected during regularization. The first pane shows the electrodes selected for the movement task in a 352 ms decoding window ending 80 ms after movement onset ($t=80$ in Figure 8), yielding 65% accuracy. The middle pane is for the same window ending at 512 ms, yielding 87% accuracy. The right pane is for vibratory stimulation, with the 352 ms window ending at 400 ms after vibration onset, and an accuracy of 96.8%.

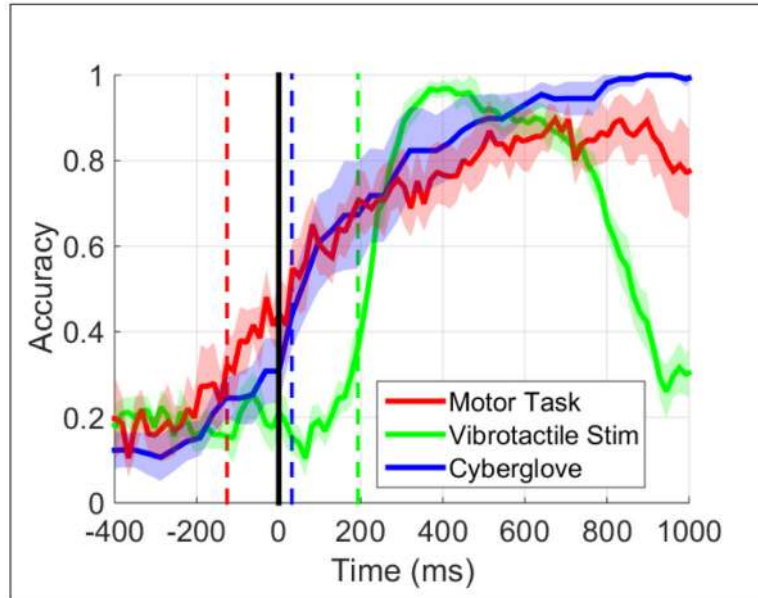


Figure 8.

Finger classification accuracy over time using CyberGlove and ECoG recordings during the motor task, and ECoG during vibrotactile stimulation. Motor task recordings are aligned to the onset of any movement by the subject's hand (solid line), and vibrotactile stimulation is aligned to onset of the vibratory motor (solid line). The red, green, and blue dashed lines denote when decoding accuracy exceeded chance levels using motor task high gamma, vibrotactile stimulation high gamma, and motor task CyberGlove data. All decoding is causal, i.e. classification accuracy at time t is dependent only on samples collected at time t and earlier. Shading represents the 95% confidence interval of the mean.

Table 1

Experimental Overview

Experiment	Purpose
Vibrotactile Stimulation	Control for sensory feedback
Finger Tapping	Two sessions: one to provide training data for our decoder, and one as an independent dataset for offline analysis
Online BMI Testing	Online test of the decoder built on finger tapping data

Author Manuscript

Author Manuscript

Author Manuscript

Author Manuscript